Water-soluble iron emitted from vehicle exhaust is linked to primary speciated organic compounds

Joseph R. Salazar*, Benton T. Cartledge*, John P. Haynes*, Rachel York-Marini*, Allen L Robinson[‡], Greg T. Drozd[€], Allen H. Goldstein[¥], Sirine C. Fakra[¢], Brian J. Majestic*

*University of Denver, Department of Chemistry and Biochemistry
[‡]Carnegie Mellon University, College of Engineering
[¥]University of California, Berkeley Department of Civil and Environmental Engineering
[€]Colby College Department of Chemistry
[¢]Advanced Light Source, Lawrence Berkeley National Laboratory, Berkeley, CA 94720

Correspondence to: Brian J. Majestic (brian.majestic@du.edu)

Abstract

Iron is the most abundant transition element in airborne PM, primarily existing as Fe(II) or Fe(III). Generally, the fraction of water-soluble iron is greater in urban areas compared to areas dominated by crustal emissions. To better understand the origin of water-soluble iron in urban areas, tail-pipe emission samples were collected from 32 vehicles with emission certifications of Tier 0, low emission vehicles (LEV I), tier two low emission vehicles (LEV II), ultralow emission vehicles (ULEV), superultra-low emission vehicles (SULEV), and partial-zero emission vehicles (PZEV). Components quantified included gases, inorganic ions, elemental carbon (EC), organic carbon (OC), total metals and water-soluble metals. Naphthalene and intermediate volatility organic compounds (IVOC) were quantified for a subset of vehicles. The IVOC quantified contained 12 to 18 carbons and were divided into three subgroups: aliphatic, single ring aromatic (SRA), and polar (material not classified as either aliphatic or SRA). Iron solubility in the tested vehicles ranged from 0 – 82% (average = 30%). X-ray absorption near edge structure (XANES) spectroscopy showed that Fe(III) was the primary oxidation state in 14 of the 16 tested vehicles, confirming that the presence of Fe(II) was not the main driver of water-soluble Fe. Correlation of water-soluble iron to sulfate was insignificant, as was correlation to

every chemical component, except to naphthalene and some C12- C18 IVOCs with R^2 values as high as 0.56. A controlled benchtop study confirmed that naphthalene, alone, increases iron solubility from soils by a factor of 5.5 and that oxidized naphthalene species are created in the extract solution. These results suggest that the large driver in water-soluble iron from primary vehicle tail-pipe emissions is related to the organic composition of the PM. We hypothesize that, during the extraction process, specific components of the organic fraction of the PM are oxidized and chelate the iron into water.

1. Introduction

Iron has been identified as a limiting nutrient for phytoplankton in approximately half of the world's oceans, with deposition from the atmosphere as the major source (Moore and Abbott, 2002; Sholkovitz et al., 2012). Phytoplankton is one of the controlling factors of fixed nitrogen in many parts of the oceans and, consequently, plays a major role in the ocean's biogeochemical cycles (Baker et al., 2006; Chen and Siefert, 2004; Kraemer, 2004; Shi et al., 2012; Tagliabue et al., 2017). Also, water-soluble iron fractions are linked to the creation of reactive oxygen species (ROS) in lung fluid and in environmental matrices through Fenton chemistry (Hamad et al., 2016). These ROS impart oxidative stress on the respiratory system, contributing to various health effects (Landreman et al., 2008; Park et al., 2006; Verma et al., 2014).

Annually, approximately 55 Tg of iron enters the atmosphere from crustal sources (Luo et al., 2008). Of this, 14-16 Tg are deposited into the ocean, impacting the marine life and influencing the ecosystems (Gao, 2003; Jickells et al., 2005). Typically, airborne iron from crustal sources ranges from 0.05-2% water-soluble of the total iron (Bonnet, 2004; Sholkovitz et al., 2012). Relative water-soluble iron in urban environments is higher, ranging from 2-50% of the total (Majestic et al., 2007; Sedwick et al., 2007; Sholkovitz et al., 2012). It is sugessted that

combustion sources including fossil fuel burning, incinerator use and biomass burning may be a large contributor to the water-soluble iron fraction, contributing 0.66-1.07 Tg a^{-1} of water-soluble iron and this iron has been correlated to anthropogenic sources (Chuang et al., 2005; Luo et al., 2008; Sholkovitz et al., 2009). From these combustion sources, it has been shown that the species of iron differed greatly and had an impact in iron solubility (Fu et al., 2012). Even though total iron emissions from combustion sources are small in comparison to crustal sources, the relative insolubility of crustal iron leads to the possibility that combustion sources contribute 20%-100% of water-soluble iron into the atmosphere (Luo et al., 2008; Sholkovitz et al., 2012).

Previous studies in tunnels and parking structures have reported iron ranging from five to approximately 3,500 ng m^{-3}, revealing that brake wear, tire wear, resuspended road dust, and tail pipe emissions can be important sources of trace elements (Kuang et al., 2017; Lawrence et al., 2013; Li and Xiang, 2013; Lough et al., 2005; Park et al., 2006; Verma et al., 2014). Iron is contained in many fuels which has pre-combusted concentrations ranging from 13-1000 μg L^{-1} (Lee and Von Lehmden, 1973; Santos et al., 2011; Teixeira et al., 2007). Within the engine, computational models of combustion in engines suggest that iron emissions could also originate from the fuel injector nozzle inside the engine block (Liati et al., 2015).

There are many different factors that may contribute to water-soluble iron and, as a result, several different hypotheses have been developed relating to how iron is solubilized in ambient atmospheres. First, correlation of ambient iron to sulfates in ambient aerosols suggest the possibility of iron solubilization (Desboeufs et al., 1999; Hand et al., 2004; Mackie et al., 2005; Oakes et al., 2012b). However, laboratory studies investigating the heterogeneous chemistry of iron have not shown any change in iron water-solubility, speciation, or oxidation state upon exposure to gaseous SO_2 (Cartledge et al., 2015; Luo et al., 2005; Majestic et al., 2007; Oakes et

al., 2012a). A second hypothesis is that particle-bound iron oxidation state may control iron water solubility. Thus far, the limited field studies have been unable to show that iron oxidation state is correlated to iron's resulting water solubility, as the majority of iron found in aerosol particles is in the less soluble Fe(III) oxidation state (Luo et al., 2005; Majestic et al., 2007; Oakes et al., 2012a). A third, broad, iron solubilization hypothesis emphasizes an iron-organic interaction (Baba et al., 2015; Vile et al., 1987). For example, a significant increase in water-soluble iron is observed in the presence of oxalate and formate in ambient aerosols and in cloud droplets (Paris et al., 2011; Zhu et al., 1993). Even when compared to sulfuric acid, oxalic acid results in a greater increase in iron solubility because of the organic iron interaction (Chen and Grassian, 2013). Other studies have suggested that the photolysis of polycyclic aromatic hydrocarbons leads to reduced iron, which may result in greater iron water solubility (Faiola et al., 2011; Haynes and Majestic, 2019; Haynes et al., 2019; Pehkonen et al., 1993; Zhu et al., 1993). Vehicle exhaust contains many organic species including secondary organic aerosol (SOA) Single-ring aromatic compounds (C6-C9) PAHs, hopanes, steranes, alkanes, organic acids and intermediate volatility organic compound (IVOCs) which are longer chain organic species (Cheung et al., 2010; Zhao et al., 2016).

In this study, we explore all three hypotheses (bulk ions, iron oxidation state, and organic speciation) in relation to iron solubility. Specifically, we examine the water-soluble iron emitted from 32 light duty gasoline vehicles with certifications of Tier 0, low emission vehicle (LEV I), tier two low emission vehicles (LEV II), ultralow emission vehicles (ULEV), superultra-low emission vehicles (SULEV), and partial-zero emission vehicles (PZEV). The total and water-soluble trace elements are compared to the ions, gaseous compounds, and organic emissions from the same vehicle set. Additionally, we acquired data on the emitted iron oxidation states on

the exhaust particles. From this data set, real tail-pipe emission samples were explored to discover how various components of automobile exhaust affect the water solubility of iron.

2. Materials and Methods

2.1. Sample Collection

Exhaust samples from 32 gasoline vehicles were collected at the California Air Resources Board (CARB) Haagen-Smit laboratory over a six-week period. Standard emission test results from this campaign have been reported previously (Saliba et al., 2017). A description of the dynamometer, emission dilution system, and instrumentation used in the vehicle set up is provided elsewhere (May et al., 2014; Saliba et al., 2017). Briefly, each vehicle was tested on a dynamometer using the cold-start Unified California (UC) Drive Cycle or the hot start Modal Arterial Cycle 4. Emission samples were collected using a constant volume sampler from which a slipstream of dilute exhaust was drawn at a flow rate of 47 L min^{-1}. Particle phase emissions were collected using three sampling trains operated in parallel off of the end of the CVS dilution tunnel. Train 1 contained a Teflon filter (47 mm, Pall-Gelman, Teflo R2PJ047). Train 2 contained two quartz filters (47 mm, Pall-Gelman, Tissuquartz 2500 QAOUP) in series. Train 3 contained an acid-cleaned Teflon filter followed by a quartz filter (47 mm, Teflo, Pall Life Sciences, Ann Arbor, MI) and the flow rate was 0.5 L min-1 through each Tenax tube. The particulate exhaust emissions were then collected on the pre-cleaned Teflon filters. The Teflon filters were stored in a freezer until extraction and analysis was performed. Filter holders were maintained at 47°C during sampling as per the CFR86 protocol.

The vehicles were recruited from private citizens, rental car agencies, or part of the Air Resource Board fleet. The vehicles tested were categorized by model years (1990-2014), vehicle type (passenger car and light-duty trucks), engine technologies (GDI and PFI), emission

123 certification standers (Tier1 to SULEV), make, and model. All vehicles were tested using the
124 same commercial gasoline fuel which had a 10 % ethanol blend and a carbon fraction of 0.82
125 (Saliba et al., 2017).

126 Gases (CO, CO_2, CH_4, NO, and NO_2) and total hydrocarbons (THC) were collected into
127 heated Tedlar bags by UC Drive Cycles. Analysis of CO and CO_2 was measured by
128 nondispersive infrared detectors (IRD-4000), CH_4 by gas chromatography, with detection by a
129 flame ionization detector (FID), NO_x by chemiluminescence (CLD 4000) and THC by FID
130 (Drozd et al., 2016; Saliba et al., 2017). The Teflon filter in Train 1 was analyzed by ion
131 chromatography for water-soluble anions and cations and procedure for these data presented
132 elsewhere (Hickox et al., 2000). Train 2 included two parallel sets of Tenax-TA sorbent tubes
133 (Gerstel) downstream of the Teflon filter. The first set was 2 tubes connected in parallel. One of
134 these tubes was used to collect emissions during the cold start phase of UC (the first five
135 minutes, commonly referred to as bag 1). The other tube was used to sample emissions during
136 the combined hot-running and hot start phases of the UC (bags 1 and 2). The second set of
137 sorbent tubes was connected in series to collect emissions over the entire UC test. The Teflo
138 filter in Train 3 was used for total and water-soluble trace element analysis and particle-bound
139 iron oxidation state and is the focus of this study.

140 2.2. Materials Preparation

141 All vessel cleaning and analytical preparation for the trace elements was performed under
142 a laminar flow hood with incoming air passing through a high efficiency particulate air (HEPA)
143 filter. All water used was purified to 18.2 MΩ-cm (Milli-Q Thermo-Fisher Nanopore). Fifteen
144 and 50 mL plastic centrifuge vials, Petri dishes (Fisher), Teflon forceps (Fisher), syringe
145 (Fisher), nitro cellulose paper (Fisher), and syringe cases (Life Sciences Products) were prepped

by an acid cleaning process. For the plastic centrifuge vials, Petri dishes, Teflon forceps, syringe, and syringe cases this involved 24-hour soaks in a 10% reagent grade nitric acid bath followed by 10% reagent grade hydrochloric bath then a 3% trace metal grade nitric acid (Fisher) resting bath with MQ rinses before, after and between each step. The nitro cellulose paper was cleaned by soaking in 2% HCl for 24 hours then rinsing with MQ water. Then, 2% HCl and MQ water were pushed through the filter. Teflon beaker liners were cleaned by an acetone rinse, then an overnight bath of 100% HPLC-grade acetonitrile and a final overnight bath of 5% trace-metal grade nitric acid. 0.20 micron syringe filters (Whatman, Marlborough, MA) were prepared with 10% trace-metal grade hydrochloric acid, MQ water and 5% nitric acid rinse.

The 47 mm Teflon filters were cleaned by submerging them in 10% trace metal grade nitric acid and rinsing with MQ water. The filters were then stored in the acid cleaned Petri dishes and sealed with Teflon tape for storage.

2.3. Water-soluble metals sample preparations

Water-soluble elements were extracted for 2 hours from the Teflon filter on a shaker table in 10 mL of MQ water. The water extract was filtered with 2 μm pore size nitro cellulose filters. The Teflon filter and the nitro cellulose filters were saved for total metals digestion. The water-soluble element extract was acidified to 5% trace-metal grade nitric acid and 2.5% trace-metal grade hydrochloric acid to be analyzed by inductively coupled plasma mass spectrometry (ICP-MS, Agilent 7700).

2.4. Sample preparation for total elemental analysis

First, ~3% (measured exactly) of the filters were cut and saved for X-ray absorption near edge structure (XANES) spectroscopy, then the water-soluble elements were extracted and,

lastly the polymethylpentene ring was removed from the Teflon filters. The Teflon and the nitro cellulose filters for each sample were placed together into a microwave digestion vessel. To each digestion vessel, 750 µL of concentrated trace metal grade nitric acid, 250 µL of concentrated trace grade hydrochloric acid, 100 µL of concentrated trace grade hydrofluoric acid, and 100 µL of 30% hydrogen peroxide was added. These samples were digested (Ethos EZ, Milestone Inc) according to the following a temperature program: 15-minute ramp to 200 °C, then held at 200 °C for 15 minutes, and a 60-minute cooling period.(Cartledge and Majestic, 2015) The samples were cooled to room temperature for 1 hour and the solution was diluted to 15 mL with MQ water and analyzed via ICP-MS.

2.5. Elemental analysis

Blank filters and standard reference materials (SRMs) were digested alongside the exhaust samples using the same digestion process described above. Three SRMs were used to address the recoveries of our digestion process: urban particulate matter (1648a, NIST), San Joaquin Soil (2709a, NIST), and Recycled Auto Catalyst (2556, NIST). The recoveries of the SRMs were between 80-120%. The elements analyzed included Na, Mg, Al, K, Ca, Ti, V, Cr, Mn, Fe, Co, Ni, Cu, Zn, As, Se, Rb, Sr, Mo, Rh, Pd, Ag, Cd, Sb, Cs, Ba, Ce, Pt, Pb, U. Indium (~1 ppb) was used as an internal standard and a He collision cell was used to remove isobaric interferences.

2.6. XANES Spectroscopy

X-ray absorption near-edge structure (XANES) and micro X-ray fluorescence (µXRF) data for 16 vehicle exhaust samples were collected at the Advanced Light Source Microprobe beamline (10.3.2), Lawrence Berkeley National Laboratory, Berkeley, CA (Marcus et al., 2004).

To locate iron spots on the filters, a broad μXRF elemental map of each sample was acquired at 10 keV using 12 μm by 12 μm pixel size and 50 ms dwell time per pixel. μXRF spectra were simultaneously recorded on each pixel of the map. Iron oxidation state and iron-bearing phases were investigated using iron K-edge extended XANES. The spectra were recorded in fluorescence mode by continuously scanning the Si (111) monochromator (Quick XAS mode) from 7011 to 7415 eV. The data were calibrated using an iron foil with first derivative set at 7110.75 eV (Kraft et al., 1996). All data were recorded using a seven-element solid state Ge detector (Canberra, ON). The spectra were deadtime corrected, deglitched, calibrated, pre-edge background subtracted and post-edge normalized using a suite of LabVIEW custom programs available at the beamline (Marcus et al., 2008). To rapidly survey iron oxidation state, a valence scatter plot was generated from normalized XANES data using a custom Matlab code and a large database of iron standards (10.3.2 XAS database) (Marcus et al., 2008). Least-square linear combination fitting (LCF) was subsequently performed in the range 7090 to 7365 eV to confirm iron valence and further identify the major mineral groups present. The best fit was chosen based on 1) minimum normalized sum-square value ($NSS=100\times[\sum(\mu_{exp}-\mu_{fit})^2/\sum(\mu_{exp})^2]$), where the addition of a spectral component to the fit required a 10% or greater improvement in the NSS value, and 2) on the elements detected in the μXRF spectrum recorded on each XANES spot. The uncertainty on the percentages of species present is estimated to be ±10%.

2.7. Organic Speciation

A subset (10) of the 32 samples were quantified for IVOC using electron impact ionization with methods similar to that of Zhao et al., except adapted for GCxGC methods (Zhao et al., 2015, 2016). IVOC material was classified into three categories: aliphatic, single ring aromatic (SRA), and polar (Drozd et al., 2019). Classification within these three classes of compounds

was determined by differences in second dimension retention time (polarity space) and by mass spectral characteristics in our GCxGC-MS analysis. All three classes of compounds were quantified by either compound specific calibration using known standards or relating total ion chromatogram (TIC) signals to calibration standards of similar volatility and polarity. In GCxGC, the TIC signal corresponds to a blob, or a region in volatility and polarity retention space. The GC-Image software package was used to create blobs from 2D chromatograms. Compounds were quantified by relating their TIC signal to that of the nearest standard in terms of polarity and volatility. Volatility bins were defined that are evenly spaced with their center elution times corresponding to each *n*-alkane. TIC blobs were quantified using the calibration for the available standard of similar polarity in the same volatility bin.

2.8. Emission Factor Calculations

Emissions data are presented as fuel-based emission factors (EF). Emission factors are calculated as the amount of analyte emitted by mass per gram of fuel emitted.

$$\mathrm{EF}_i(g\ g-fuel^{-1}) = \Delta m_i \frac{x_c(g)}{\Delta \mathrm{CO}_2(g) + \Delta \mathrm{CO}(g) + \Delta \mathrm{THC}(g)}$$

ΔCO_2, ΔCO, and ΔTHC are the background corrected carbon concentration of CO_2, CO, and THC (Drozd et al., 2016; Goldstein et al., 2017), respectively. x_c is the fuel carbon mass fraction of 0.82. Δm_i is the blank subtracted concentrations of species *i*.

2.9. Naphthalene and Iron Benchtop Study

To better understand the production of soluble iron during the water extraction process, a bench-top study was performed using three varying forms of iron with naphthalene. The iron stock solutions/suspensions included: 1) standardized San Joaquin soil (NIST SRM 2709a)

containing 25 ppm total iron (soluble + insoluble) iron to determine the effects of crustal iron, 2) iron(II) sulfate to a concentration of 25 ppm to examine the effect of a soluble iron(II) source, and 3) iron(III) sulfate to examine a source of soluble iron(III). In parallel, 100 mg of naphthalene crystals were added to 200 mL of MQ water. For the experiment, 99 mL of the naphthalene suspension and 1 mL of the iron suspension were added to Teflon liners (250 ppb iron total), which were inserted into a jacked glass beaker temperature controlled to 25 °C. After 16 hr of stirring, 2 ml were filtered (0.2 µm) and acidified to 5% nitric acid. Soluble iron released from the soil both in the presence and absence of naphthalene was analyzed by ICP-MS. Chemical changes in naphthalene in the presence and absence of iron were monitored by HPLC.

3. Results and Discussion

3.1. Total and water-soluble element exhaust concentrations

Table 1:

Emissions of ions, organic species, gaseous species, and EC/OC from these tests have been published previously (Drozd et al., 2016, 2019; Goldstein et al., 2017; Saliba et al., 2017). In order to obtain a better understanding of the factors that influence iron solubility, we compare these with the total elements, trace elements, and iron oxidation state measurements. Generally, the elements with the highest EF are the lighter crustal elements Ca, Al, and Fe, with average EF 200, 100, and 80 µg kg-fuel^{-1} (Table 1), respectively. Iron has the third highest average EF of all the elements and the highest of all transition elements, ranging from 0 – 200 µg Fe kg-fuel^{-1}. This is followed by three first row transition elements: Zn, Cu, and Ni with the respective average EF of 60, 20, and 5 µg kg-fuel^{-1}. Other notable elements include Rh, Pd and Pt, likely originating from the catalytic convertor, with the respective average EF of 0.05, 0.7, and 0.04 µg

kg-fuel^{-1}. Toxic elements include Chromium, Lead, Molybdenum and Antimony with respective EF 5, 0.8, 5 and 0.2 µg kg-fuel^{-1}. A previous study has shown that various elements are enriched in used motor oil such as copper, zinc, manganese, iron and lead which could originate from engine wear (Majestic et al., 2009).

Table 1 also shows the EF for the water-soluble fraction of the trace elements. The water-soluble EF for iron ranges from 0-150 µg kg-fuel^{-1}; or 0-82% of the total. At 20 µg kg-fuel^{-1}, average water-soluble iron was the third largest EF of all elements. There were relatively high emissions of a few other water-soluble elements such as Ca with an average EF of 200 µg kg-fuel^{-1} and Zn with tailpipe emissions averaging 40 µg kg-fuel^{-1}.

Table 2:

Only a few studies report tailpipe emissions (i.e., dynamometer testing) of trace elements for diesel and gasoline-powered passenger cars and even fewer which have reported iron water Table 2 compares the average exhaust PM composition and trace elements in distance-based emission factors in this study to literature values for other passenger vehicles, including one diesel and three gasoline exhaust studies. For all elements, the distance-based emission factors were greater in the diesel cohort, relative to the gasoline vehicles. Compared to previous studies, the trace elements emitted from older gasoline passenger vehicles resulted in an order of magnitude higher emissions for all elements, except for aluminum, which only showed a factor of ~2 increase in older vehicles (Table 2). Iron shows a large range in the three studies of gasoline vehicles, ranging from 8.3-280 µg km^{-1}, compared to the 0-62 µg km^{-1} measured in this study.

Figure 1:

278 Figure 2:

279 The large ranges in iron solubility of the previous studies led us to explore and compare
280 the newer emission certification standard (Figure 1 and 2). Total iron did not trend strongly with
281 emission certification standard, although, on average, total iron is less in the Tier 0 and LEV
282 vehicles. Water-soluble iron shows a small average decrease of approximately 5 µg kg-fuel^{-1}
283 between ULEV and SULEV vehicles, and a further average decrease for the PZEV vehicles of
284 3.9 µg kg-fuel^{-1}.

285 *3.2. Iron correlations with bulk exhaust components and iron oxidation state*

286 Figure 3:

287 To explore what factors and if any exhaust components are associated with the presence
288 of water-soluble iron, linear regression analyses were used to compare soluble iron to different
289 chemical species in the exhaust. Solubility from the direct exhaust was explored by comparing
290 the EFs of both sulfate and nitrate to iron, and water-soluble iron was not correlated to either of
291 these species (SI1 and Figure 3). The EFs for water-soluble iron and CO_2 showed no correlation,
292 suggesting that overall fuel use was not an important factor for water-soluble iron production
293 (SI1). Total iron was correlated to the water-soluble iron indicating the total amount of iron may
294 have an impact on soluble iron (SI2). Finally, to evaluate if water-soluble iron and overall
295 particulate carbon relate, the EFs for elemental carbon (EC) and organic carbon (OC) were
296 compared to that of soluble iron and, again, no correlation was observed (SI1 and Figure 3).

297 Figure 4:

298 As no correlation between water-soluble iron and bulk chemical species was observed
299 (SI1 and SI3), the importance of the particle-bound iron oxidation state was investigated. Since

Fe(II) is known to be more soluble than Fe(III), the expectation was that exhaust samples having a large Fe(II) character would have a greater iron solubility, relative to those containing Fe(III) or to Fe(0) (Stumm and Morgan, 1996). Figure 3 presents a scatter plot of the iron valence in 16 of the exhaust samples, compared with iron-bearing standards of known valence. This valence plot is generated from iron K-edge XANES data where parameters κ and μ are defined as normalized absorbance values at 7113 eV and 7117.5 eV, respectively. We observe that the exhaust-iron is primarily in the Fe(III) oxidation state, except for two vehicles: sample 11, dominated by Fe(0) and sample 15, containing a combination of Fe(0) and Fe(III) (SI4). Sample 11 is an extreme case, having 0 % iron solubility and highly elevated amount of EC at 305 μg kg-fuel^{-1} (study average = 78 μg kg-Fuel^{-1}). The presence of Fe(0) is consistent with high EC, as both observations suggest a lack of oxidation during the combustion and emission process. While the valence plot (Figure 3) put sample 15 as mostly Fe(II), the LCF actually showed that it was a mixture of Fe(0) and Fe(III). And, this sample contained only 10% water-soluble iron, less than the cohort average. The study-wide solid phase iron oxidation state is primarily Fe(III) or mixed oxidation state (Fe(III) and Fe(0)) (see Figure 3), averaging about 30% water-soluble iron, well above the crustal background.

LCF XANES fitting (SI4) showed Fe(III) oxides and oxyhydroxides as the dominant group, followed by Fe(III) sulfates and iron silicates (SI4). Hematite (α-Fe_2O_3) and maghemite (γ-Fe_2O_3) were the most consistently detected Fe(III) oxides. Iron was detected in all samples, with Zn, Cr and Cu the main other elements detected in nearly all samples (detection of low-Z elements below sulfur or high-Z elements above zinc was not possible in our experimental conditions). Overall, these results strongly suggest that the main driver of water-soluble iron is not associated with the particle-bound iron oxidation state. Further investigation for the LCF

XANES fitting showed that 34% of iron speciated was Fe(III)-oxyhydroxides associated with organic material leading to the investigation of organic species which resulted in a correlation to longer chain IVOC and naphthalene (SI6).

3.3. Iron solubility and speciated organics

Figure 5

Finally, the relationship between water-soluble iron and speciated organics, specifically naphthalene and IVOCs, was examined. In contrast with all other measured parameters, Figure 4 shows relatively strong correlations between water-soluble iron and some of the IVOC species. Figure 4 presents the classifications which have the strongest correlation with water-soluble iron. Water-soluble iron relationships with other IVOCs can be found in the supplementary information (SI8). The correlation to water-soluble iron is highest for IVOC-polar species with 16 carbons ($R^2 = 0.56$). The variance of figure 4 could result from the fact that, in addition to the IVOCs, other factors also influence iron water solubility.

As water-soluble iron trends well with naphthalene and polar-IVOCs, but not with bulk EC or OC, it is highly suggestive that iron solubility from the direct emission samples is primarily dependent on interactions with the species of carbon present in the particles during the extraction process. To better understand these interactions, a preliminary laboratory study was conducted to explore both i) the effect of these organic compounds on iron solubility and ii) the effect of soluble iron on the oxidation of organic compounds during the extraction process. Specifically, when naphthalene was added to an insoluble iron source (a soil), iron solubility increased from 0.8 to 4.2 % of the total, or by a factor of ~5.5, showing that the addition of

344 naphthalene, alone, can have a significant effect on iron water solubility and that this effect
345 likely is important during the extraction process.

346 Figure 6:

347 Lacking oxidized functional groups, naphthalene was not expected to chelate iron or to,
348 otherwise, have the ability to increase iron solubility. Thus, we investigated what compounds are
349 formed from naphthalene during these extractions. Figure 5 shows the new oxidized products
350 formed from naphthalene during the water extraction. In the presence of soluble iron, HPLC
351 retention time analysis shows the presence of phthalic acid (12.5 minutes), phthalic anhydride
352 (7.5 minutes), and naphthol (15 minutes). The peaks at and below 5 min were not identified but,
353 based on the retention times, these are thought to be low molecular mass, highly polar organic
354 products and is consistent with other studies (Haynes et al., 2019)

355 *3.4. Iron-carbon interactions*

356 There are at least two methods in which organic compounds can lead to increased iron
357 solubility: a) reduction of Fe(III) to Fe(II) or b) bringing soluble iron into solution via chelation.
358 The first one is generally achieved by photochemistry (Pehkonen et al., 1993), which is not
359 directly applicable to this study. The second, chelation, generally requires oxidized functional
360 groups as shown in Figure 5. The extent of the ability for phthalic acid (a dicarboxylic acid) to
361 chelate iron has not been reported, however, it is known that similar molecular mass organic
362 diacids have significant ability to chelate iron, thus pulling it into solution (Paris and Desboeufs,
363 2013). Here, we suggest that the observed correlations between IVOC/naphthalene and water-
364 soluble iron can be best explained with Fenton reactions, resulting in propagation of radical
365 reactions (Pehkonen et al., 1993). As shown from the Fe XANES valance plot, the iron is
366 predominately Fe(III) (Figure 4). In addition to the Fe(III), it has been shown that H_2O_2 forms in

367 $PM_{2.5}$ water extracts and it been speculated that this formation is from various transition metals
368 and/or quinones found in $PM_{2.5}$ (Wang et al., 2012).

369 $$Fe^{3+} + H_2O_2 \rightarrow Fe^{2+} + H^+ + HO_2^{\circ} \quad (1)$$

370 $$HO_2^{\circ} \rightarrow H^+ + O_2^{\circ -} \quad (2)$$

371 $$H^+ + O_2^{\circ -} + Naphthalene \rightarrow Oxidized\ Naphthalene \quad (3)$$

372

373 In the presence of H_2O_2, Fe(III) is known to undergo reaction (1) (Neyens and Baeyens,
374 2003; Pignatello et al., 2006), resulting in the formation of Fe(II) and HO_2 (Pignatello et al.,
375 2006; Rubio-Clemente et al., 2014), which degrades into superoxide, O_2^-, and H^+ (2). Superoxide
376 has the ability to oxidize organic compounds, particularly aromatic structures (3) (Lair et al.,
377 2008). The resulting structures of these oxidized compounds typically have two oxygen atoms,
378 which could be arranged in various functional groups (Lair et al., 2008; Rubio-Clemente et al.,
379 2014), also observed from the HPLC chromatograms. Oxidized single ring aromatic structures
380 have a strong affinity to iron and have the ability chelate iron into aqueous solution (Haynes and
381 Majestic, 2019; Hosseini and Madarshahian, 2009). Based on the laboratory studies of
382 naphthalene and soluble-iron presented here, naphthalene and/or IVOC oxidation during the
383 extraction process is the most likely path towards increased iron solubility in primary tailpipe
384 emissions. This overall process suggests that Fe(III) is emitted though car exhaust though
385 interaction with water and organics undergoes a Fenton like reaction and converted to Fe(II) and
386 the iron is chelated by the resulting oxidized organics.

387 ## 4. Conclusions

388 This study shows water-soluble iron is directly formed from vehicle exhaust and not
389 correlated to sulfates. The results show that iron is solubilized in water by specific organic

compounds present in automobile exhaust, and that soluble iron is not necessarily dictated by the overall OC content. Thus, the implication is that anthropogenic water-soluble iron is a result of chelation from specific organic compounds, likely their eventual aqueous reaction products. Although the mechanism of these aqueous transformations were not directly measured in this study, based on Fenton chemistry, the primary compounds are expected to be oxidized versions of naphthalene and/or IVOCs (Ledakowicz et al., 1999). Since these oxidation reactions occur fairly quickly (i.e., during the water extraction), further studies are of interest to better understand how these organic compounds interact with iron as it enters atmospheric waters and, also, the photo-chemical interactions between iron and organics.

Acknowledgements

The authors thank the excellent and dedicated personnel at the California Air Resources Board, especially at the Haagen–Smit Laboratory. This study was funded by National Science Foundation grant numbers 1342599 and 1549166. This research used resources of the Advanced Light Source, which is a DOE Office of Science User Facility under contract no. DE-AC02-05CH11231. Financial support was provided by the California Air Resources Board (Contract #12-318). The California Air Resources Board also provided substantial in-kind support for vehicle procurement, testing, and emissions characterization.

Author contribution

The sample collection scheme was designed by Allen L. Robinson, Allen H. Goldstein and Brian J. Majestic. Samples were collected by Benton T. Cartledge and Greg T. Drozd. Organic speciation was performed by Greg T. Drozd. Trace elements were quantified by Joseph R. Salazar. Iron speciation was performed by Joseph R. Salazar, Rachel York-Marini and Brian

J. Majestic, with the interpretation effort led by Sirine C. Fakra. Bench-top naphthene experiments were performed by John P. Haynes. Data integration was performed by Joseph R. Salazar. The manuscript was prepared by Joseph R. Salazar and Brian J. Majestic.

References

Baba, Y., Yatagai, T., Harada, T. and Kawase, Y.: Hydroxyl radical generation in the photo-fenton process: Effects of carboxylic acids on iron redox cycling, Chem. Eng. J., 277, 229–241, doi:10.1016/j.cej.2015.04.103, 2015.

Baker, A. R., Jickells, T. D., Witt, M. and Linge, K. L.: Trends in the solubility of iron, aluminium, manganese and phosphorus in aerosol collected over the Atlantic Ocean, Mar. Chem., 98(1), 43–58, doi:10.1016/j.marchem.2005.06.004, 2006.

Bonnet, S.: Dissolution of atmospheric iron in seawater, Geophys. Res. Lett., 31(3), L03303, doi:10.1029/2003GL018423, 2004.

Cartledge, B. T. and Majestic, B. J.: Metal concentrations and soluble iron speciation, Atmos. Pollut. Res., (6), 495–505, 2015.

Cartledge, B. T., Marcotte, A. R., Herckes, P., Anbar, A. D. and Majestic, B. J.: The Impact of Particle Size, Relative Humidity, and Sulfur Dioxide on Iron Solubility in Simulated Atmospheric Marine Aerosols, Environ. Sci. Technol., 49(12), 7179–7187, doi:10.1021/acs.est.5b02452, 2015.

Chen, Y. and Siefert, R. L.: Seasonal and spatial distributions and dry deposition fluxes of atmospheric total and labile iron over the tropical and subtropical North Atlantic Ocean, J. Geophys. Res. D Atmos., 109(9), doi:10.1029/2003JD003958, 2004.

Cheung, K. L., Ntziachristos, L., Tzamkiozis, T., Schauer, J. J., Samaras, Z., Moore, K. F. and Sioutas, C.: Emissions of particulate trace elements, metals and organic species from gasoline, diesel, and biodiesel passenger vehicles and their relation to oxidative potential, Aerosol Sci.

452 Technol., 44(7), 500–513, doi:10.1080/02786821003758294, 2010.

453 Chuang, P. Y., Duvall, R. M., Shafer, M. M. and Schauer, J. J.: The origin of water soluble
454 particulate iron in the Asian atmospheric outflow, Geophys. Res. Lett., 32(7), 1–4,
455 doi:10.1029/2004GL021946, 2005.

456 Desboeufs, K. V, Losno, R. and Cholbi, S.: The pH-dependent dissolution of wind-transported, ,
457 104, 1999.

458 Drozd, G. T., Zhao, Y., Saliba, G., Frodin, B., Maddox, C., Weber, R. J., Chang, M. C. O.,
459 Maldonado, H., Sardar, S., Robinson, A. L. and Goldstein, A. H.: Time Resolved Measurements
460 of Speciated Tailpipe Emissions from Motor Vehicles: Trends with Emission Control
461 Technology, Cold Start Effects, and Speciation, Environ. Sci. Technol., 50(24), 13592–13599,
462 doi:10.1021/acs.est.6b04513, 2016.

463 Drozd, G. T., Zhao, Y., Saliba, G., Frodie, B., Maddox, C., Chang, M.-C. O., Maldonado, H.,
464 Sardar, S., Weber, R. J., Robinson, A. L. and Goldstein, A. H.: Detailed Speciation of
465 Intermediate Volatility and Semivolatile Organic Compound Emissions from Gasoline Vehicles:
466 Effects of Cold-Starts and Implications for Secondary Organic Aerosol Formation., Environ. Sci.
467 Technol., 53(3), 1706–1714, 2019.

468 Faiola, C., Johansen, A. M., Rybka, S., Nieber, A., Thomas, C., Bryner, S., Johnston, J.,
469 Engelhard, M., Nachimuthu, P. and Owens, K. S.: Ultrafine particulate ferrous iron and
470 anthracene associations with mitochondrial dysfunction, Aerosol Sci. Technol., 45(9), 1109–
471 1122, doi:10.1080/02786826.2011.581255, 2011.

472 Gao, Y.: Aeolian iron input to the ocean through precipitation scavenging: A modeling
473 perspective and its implication for natural iron fertilization in the ocean, J. Geophys. Res.,

108(D7), 4221, doi:10.1029/2002JD002420, 2003.

Goldstein, A., Robinson, A., Kroll, J., Drozd, G., Zhao, Y., Saliba, G., Saleh, R. and Presto, A.: Investigating Semi-Volatile Organic Compound Emissions from Light-Duty Vehicles., 2017.

Hamad, S. H., Schauer, J. J., Antkiewicz, D. S., Shafer, M. M. and Kadhim, A. K. H.: ROS production and gene expression in alveolar macrophages exposed to PM2.5 from Baghdad, Iraq: Seasonal trends and impact of chemical composition, Sci. Total Environ., 543, 739–745, doi:10.1016/j.scitotenv.2015.11.065, 2016.

Hand, J. L., Mahowald, N. M., Chen, Y., Siefert, R. L., Luo, C., Subramaniam, A. and Fung, I.: Estimates of atmospheric-processed soluble iron from observations and a global mineral aerosol model: Biogeochemical implications, J. Geophys. Res. D Atmos., 109(17), 1–21, doi:10.1029/2004JD004574, 2004.

Haynes, J. and Majestic, B.: Role of polycyclic aromatic hydrocarbons on the photo-catalyzed solubilization of simulated soil-bound atmospheric iron, Atmos. Pollut. Res., doi:https://doi.org/10.1016/j.apr.2019.12.007, 2019.

Haynes, J. P., Miller, K. E. and Majestic, B. J.: Investigation into Photoinduced Auto-Oxidation of Polycyclic 2 Aromatic Hydrocarbons Resulting in Brown Carbon Production, Environ. Sci. Technol., 53(3), 10.1021/acs.est.8b05704, doi:10.1021/acs.est.8b05704, 2019.

Hickox, W. H., Werner, B. and Gaffney, P.: Air Resources Board, , (Mld), 1–6 [online] Available from: http://www.arb.ca.gov/ei/see/memo_ag_emission_factors.pdf, 2000.

Hosseini, M. S. and Madarshahian, S.: Investigation of charge transfer complex formation between Fe(III) and 2,6-Dihydroxy benzoic acid and its applications for spectrophotometric

495 determination of iron in aqueous media, E-Journal Chem., 6(4), 985–992,
496 doi:10.1155/2009/417303, 2009.

497 Jickells, T. D., An, Z. S., Andersen, K. K., Baker, a R., Bergametti, G., Brooks, N., Cao, J. J.,
498 Boyd, P. W., Duce, R. a, Hunter, K. a, Kawahata, H., Kubilay, N., LaRoche, J., Liss, P. S.,
499 Mahowald, N., Prospero, J. M., Ridgwell, a J., Tegen, I. and Torres, R.: Global iron connections
500 between desert dust, ocean biogeochemistry, and climate., Science, 308(5718), 67–71,
501 doi:10.1126/science.1105959, 2005.

502 Kraemer, S. M.: Iron oxide dissolution and solubility in the presence of siderophores, Aquat.
503 Sci., 66(1), 3–18, doi:10.1007/s00027-003-0690-5, 2004.

504 Kraft, S., Stümpel, J. and Becker, P.: High resolution x-ray absorption spectroscopy with
505 absolute energy calibration for the determination of absorption edge energiestle, Rev. Sci.
506 Instrum., 67, 681, 1996.

507 Kuang, X. M., Scott, J. A., da Rocha, G. O., Betha, R., Price, D. J., Russell, L. M., Cocker, D. R.
508 and Paulson, S. E.: Hydroxyl radical formation and soluble trace metal content in particulate
509 matter from renewable diesel and ultra low sulfur diesel in at-sea operations of a research vessel,
510 Aerosol Sci. Technol., 51(2), 147–158, doi:10.1080/02786826.2016.1271938, 2017.

511 Lair, A., Ferronato, C., Chovelon, J. M. and Herrmann, J. M.: Naphthalene degradation in water
512 by heterogeneous photocatalysis: An investigation of the influence of inorganic anions, J.
513 Photochem. Photobiol. A Chem., 193(2–3), 193–203, doi:10.1016/j.jphotochem.2007.06.025,
514 2008.

515 Landreman, A. P., Shafer, M. M., Hemming, J. C., Hannigan, M. P. and Schauer, J. J.: A
516 Macrophage-Based Method for the Assessment of the Reactive Oxygen Species (ROS) Activity

517 of Atmospheric Particulate Matter (PM) and Application to Routine (Daily-24 h) Aerosol
518 Monitoring Studies, Aerosol Sci. Technol., 42(11), 946–957, doi:10.1080/02786820802363819,
519 2008.

520 Lawrence, S., Sokhi, R., Ravindra, K., Mao, H., Prain, H. D. and Bull, I. D.: Source
521 apportionment of traffic emissions of particulate matter using tunnel measurements, Atmos.
522 Environ., 77, 548–557, doi:10.1016/j.atmosenv.2013.03.040, 2013.

523 Ledakowicz, S., Miller, J. S. and Olejnik, D.: Oxidation of PAHs in water solutions by
524 ultraviolet radiation combined with hydrogen peroxide, Int. J. Photoenergy, 1(1), 1–6,
525 doi:10.1155/S1110662X99000100, 1999.

526 Li, Y. and Xiang, R.: Particulate pollution in an underground car park in Wuhan, China,
527 Particuology, 11(1), 94–98, doi:10.1016/j.partic.2012.06.010, 2013.

528 Lough, G. C., Schauer, J. J., Park, J. S., Shafer, M. M., Deminter, J. T. and Weinstein, J. P.:
529 Emissions of metals associated with motor vehicle roadways, Environ. Sci. Technol., 39(3), 826–
530 836, doi:10.1021/es048715f, 2005.

531 Luo, C., Mahowald, N. M., Meskhidze, N., Chen, Y., Siefert, R. L., Baker, A. R. and Johansen,
532 A. M.: Estimation of iron solubility from observations and a global aerosol model, J. Geophys.
533 Res. Atmos., 110(23), 1–23, doi:10.1029/2005JD006059, 2005.

534 Luo, C., Mahowald, N., Bond, T., Chuang, P. Y., Artaxo, P., Siefert, R., Chen, Y. and Schauer,
535 J.: Combustion iron distribution and deposition, Global Biogeochem. Cycles, 22,
536 doi:10.1029/2007GB002964, 2008.

537 Mackie, D. S., Boyd, P. W., Hunter, K. A. and McTainsh, G. H.: Simulating the cloud processing

of iron in Australian dust: pH and dust concentration, Geophys. Res. Lett., 32(6), 1–4, doi:10.1029/2004GL022122, 2005.

Majestic, B. J., Schauer, J. J. and Shafer, M. M.: Application of synchrotron radiation for measurement of iron red-ox speciation in atmospherically processed aerosols, Atmos. Chem. Phys. Atmos. Chem. Phys., 7(Iii), 2475–2487, doi:10.5194/acpd-7-1357-2007, 2007.

Majestic, B. J., Anbar, A. D. and Herckes, P.: Elemental and iron isotopic composition of aerosols collected in a parking structure, Sci. Total Environ., 407(18), 5104–5109, doi:10.1016/j.scitotenv.2009.05.053, 2009.

Marcus, M. A., Macdowell, A. A., Celestre, R., Manceau, A., Miller, T., Padmore, H. A. and Sublett, R. E.: Beamline 10.3.2 at ALS: a hard X-ray microprobe for environmental and materials sciences, J. Synchrotron Radiat., 11, 239–247, doi:10.1107/S0909049504005837, 2004.

Marcus, M. A., Westphal, A. J. and Fakra, S. C.: Classification of Fe-bearing species from K-edge XANES data using two-parameter correlation plots, J. Synchrotron Radiat., 15(5), 463–468, doi:10.1107/S0909049508018293, 2008.

May, A. A., Nguyen, N. T., Presto, A. A., Gordon, T. D., Lipsky, E. M., Karve, M., Gutierrez, A., Robertson, W. H., Zhang, M., Brandow, C., Chang, O., Chen, S., Cicero-Fernandez, P., Dinkins, L., Fuentes, M., Huang, S. M., Ling, R., Long, J., Maddox, C., Massetti, J., McCauley, E., Miguel, A., Na, K., Ong, R., Pang, Y., Rieger, P., Sax, T., Truong, T., Vo, T., Chattopadhyay, S., Maldonado, H., Maricq, M. M. and Robinson, A. L.: Gas- and particle-phase primary emissions from in-use, on-road gasoline and diesel vehicles, Atmos. Environ., 88, 247–260, doi:10.1016/j.atmosenv.2014.01.046, 2014.

560 Moore, J. K. and Abbott, M. R.: Surface chlorophyll concentrations in relation to the Antarctic
561 Polar Front: Seasonal and spatial patterns from satellite observations, J. Mar. Syst., 37(1–3), 69–
562 86, doi:10.1016/S0924-7963(02)00196-3, 2002.

563 Neyens, E. and Baeyens, J.: A review of classic Fenton's peroxidation as an advanced oxidation
564 technique, J. Hazard. Mater., 98(1–3), 33–50, doi:10.1016/S0304-3894(02)00282-0, 2003.

565 Norbeck, J. M., Durbin, T. D. and Truex, T. J.: Measurement of primary particulate matter
566 emissions from light-duty motor vehicles, Riverside., 1998.

567 Oakes, M., Weber, R. J., Lai, B., Russell, A. and Ingall, E. D.: Characterization of iron
568 speciation in urban and rural single particles using XANES spectroscopy and micro X-ray
569 fluorescence measurements: Investigating the relationship between speciation and fractional iron
570 solubility, Atmos. Chem. Phys., 12(2), 745–756, doi:10.5194/acp-12-745-2012, 2012a.

571 Oakes, M., Ingall, E. D., Lai, B., Shafer, M. M., Hays, M. D., Liu, Z. G., Russell, A. G. and
572 Weber, R. J.: Iron solubility related to particle sulfur content in source emission and ambient fine
573 particles, Environ. Sci. Technol., 46(12), 6637–6644, doi:10.1021/es300701c, 2012b.

574 Paris, R. and Desboeufs, K. V.: Effect of atmospheric organic complexation on iron-bearing dust
575 solubility, Atmos. Chem. Phys., 13(9), 4895–4905, doi:10.5194/acp-13-4895-2013, 2013.

576 Paris, R., Desboeufs, K. V. and Journet, E.: Variability of dust iron solubility in atmospheric
577 waters: Investigation of the role of oxalate organic complexation, Atmos. Environ., 45(36),
578 6510–6517, doi:10.1016/j.atmosenv.2011.08.068, 2011.

579 Park, S., Nam, H., Chung, N., Park, J.-D. and Lim, Y.: The role of iron in reactive oxygen
580 species generation from diesel exhaust particles, Toxicol. Vitr., 20(6), 851–857,

581 doi:10.1016/j.tiv.2005.12.004, 2006.

582 Pehkonen, S. O., Siefert, R., Erel, Y., Webb, S. and Hoffmann, M. R.: Photoreduction of Iron
583 Oxyhydroxides in the Presence of Important Atmospheric Organic Compounds, Environ. Sci.
584 Technol., 27(10), 2056–2062, doi:10.1021/es00047a010, 1993.

585 Pignatello, J. J., Oliveros, E. and MacKay, A.: Advanced oxidation processes for organic
586 contaminant destruction based on the fenton reaction and related chemistry, Crit. Rev. Environ.
587 Sci. Technol., 36(1), 1–84, doi:10.1080/10643380500326564, 2006.

588 Rubio-Clemente, A., Torres-Palma, R. A. and Peñuela, G. A.: Removal of polycyclic aromatic
589 hydrocarbons in aqueous environment by chemical treatments: A review, Sci. Total Environ.,
590 478, 201–225, doi:10.1016/j.scitotenv.2013.12.126, 2014.

591 Saliba, G., Saleh, R., Zhao, Y., Presto, A. A., Lambe, A. T., Frodin, B., Sardar, S., Maldonado,
592 H., Maddox, C., May, A. A., Drozd, G. T., Goldstein, A. H., Russell, L. M., Hagen, F. and
593 Robinson, A. L.: Comparison of Gasoline Direct-Injection (GDI) and Port Fuel Injection (PFI)
594 Vehicle Emissions: Emission Certification Standards, Cold-Start, Secondary Organic Aerosol
595 Formation Potential, and Potential Climate Impacts, Environ. Sci. Technol., 51(11), 6542–6552,
596 doi:10.1021/acs.est.6b06509, 2017.

597 Schauer, J. J., Kleeman, M. J., Cass, G. R. and Simoneit, B. R. T.: Measurement of emissions
598 from air pollution sources. 5. C1-C32 organic compounds from gasoline-powered motor
599 vehicles., Environ. Sci. Technol., 36(6), 1169–1180, doi:10.1021/es0108077, 2002.

600 Sedwick, P. N., Sholkovitz, E. R. and Church, T. M.: Impact of anthropogenic combustion
601 emissions on the fractional solubility of aerosol iron: Evidence from the Sargasso Sea,
602 Geochemistry, Geophys. Geosystems, 8(10), doi:10.1029/2007GC001586, 2007.

Shi, Z., Krom, M. D., Jickells, T. D., Bonneville, S., Carslaw, K. S., Mihalopoulos, N., Baker, A. R. and Benning, L. G.: Impacts on iron solubility in the mineral dust by processes in the source region and the atmosphere: A review, Aeolian Res., 5, 21–42, doi:10.1016/j.aeolia.2012.03.001, 2012.

Sholkovitz, E. R., Sedwick, P. N. and Church, T. M.: Influence of anthropogenic combustion emissions on the deposition of soluble aerosol iron to the ocean: Empirical estimates for island sites in the North Atlantic, Geochim. Cosmochim. Acta, 73(14), 3981–4003, doi:10.1016/j.gca.2009.04.029, 2009.

Sholkovitz, E. R., Sedwick, P. N., Church, T. M., Baker, A. R. and Powell, C. F.: Fractional solubility of aerosol iron: Synthesis of a global-scale data set, Geochim. Cosmochim. Acta, 89, 173–189, doi:10.1016/j.gca.2012.04.022, 2012.

Stumm, W. and Morgan, J. J.: Aquatic Chemistry: Chemical Equilibria and Rates in Natural Waterse, 3rd ed., Wiley-Interscience., 1996.

Tagliabue, A., Bowie, A. R., Philip, W., Buck, K. N., Johnson, K. S. and Saito, M. A.: Review The integral role of iron in ocean biogeochemistry, Nat. Publ. Gr., 543(7643), 51–59, doi:10.1038/nature21058, 2017.

Verma, V., Fang, T., Guo, H., King, L., Bates, J. T., Peltier, R. E., Edgerton, E., Russell, A. G. and Weber, R. J.: Reactive oxygen species associated with water-soluble PM2.5 in the southeastern United States: Spatiotemporal trends and source apportionment, Atmos. Chem. Phys., 14(23), 12915–12930, doi:10.5194/acp-14-12915-2014, 2014.

Vile, G. F., Winterbourn, C. C. and Sutton, H. C.: Radical-driven fenton reactions: Studies with paraquat, adriamycin, and anthraquinone 6-sulfonate and citrate, ATP, ADP, and pyrophosphate

iron chelates, Arch. Biochem. Biophys., 259(2), 616–626, doi:10.1016/0003-9861(87)90528-5, 1987.

Wang, Y., Arellanes, C. and Paulson, S. E.: Hydrogen peroxide associated with ambient fine-mode, diesel, and biodiesel aerosol particles in Southern California, Aerosol Sci. Technol., 46(4), 394–402, doi:10.1080/02786826.2011.633582, 2012.

Zhao, Y., Nguyen, N. T., Presto, A. A., Hennigan, C. J., May, A. A. and Robinson, A. L.: Intermediate Volatility Organic Compound Emissions from On-Road Diesel Vehicles: Chemical Composition, Emission Factors, and Estimated Secondary Organic Aerosol Production, Env. Sci. Tech., 49, 11516–11526, doi:10.1021/acs.est.5b02841, 2015.

Zhao, Y., Nguyen, N. T., Presto, A. A., Hennigan, C. J., May, A. A. and Robinson, A. L.: Intermediate Volatility Organic Compound Emissions from On-Road Gasoline Vehicles and Small Off-Road Gasoline Engines., Environ. Sci. Technol., 50, 4554–4563, doi:10.1021/acs.est.5b06247, 2016.

Zhu, X., Prospero, J. M., Savoie, D. L., Millero, F. J., Zika, R. G. and Saltzman, E. S.: Photoreduction of iron(III) in marine mineral aerosol solutions, J. Geophys. Res. Atmos., 98(D5), 9039–9046, doi:10.1029/93JD00202, 1993.

Tables and Figures and Captions

Figure 1: Total iron from the 32 vehicles tested reported in EF (μg kg-fuel^{-1}). The center black line represents the median value and the edges of the boxes represent the 25th and 75th percentiles while the whiskers extent are the 10th and 90th percentiles.

Figure 2: Water-soluble iron from the 32 vehicles tested reported in water-soluble iron fraction. The center black line represents the median value and the edges of the boxes represent the 25th and 75th percentiles while the whiskers are the 10th and 90th percentiles.

Figure 3: Linear correlation plots representing EF in mg kg-fuel-1 for sulfate and organic carbon (OC) in μg kg-fuel^{-1} for water-soluble iron. Correlation lines and R2 values for all elements are shown.

Figure 4: Fe valence scatter plot generated from Fe K-edge XANES data where κ and μ are normalized absorbance values at 7113 eV and 7117.5 eV respectively. Empty black squares represent Fe standards of known valence while blue-filled stars represent vehicle exhaust samples.

Figure 5: Scatter plots of water-soluble iron versus the sum of IVOCs reported in EF (g kg-fuel^{-1}).

Figure 6: HPLC of resulting reaction between naphthalene and water-soluble iron. Phathalic acid at 12.5 minutes, phthalic anyhydride at 7.5 minutes, napthol at 15 minutes and naphthalene at 20 minutes. The column uses a C18 stationary phase on beads with 80Å pore size.

665 Table 1: Average of total trace total and water soluble elements from car exhaust reported in EF
666 (μg kg-fuel^{-1}). These samples represent a range of different makes and models of cars. The
667 values in the parenthesis are the range of the vehicle populualtion. (n=32)

668 Table 2: Comparison of exhaust composition in g km^{-1} from different dynamometer studies
669 which included both gasoline and diesel powered light duty vehicles. The values are the mean of
670 the vehicle population and the values in the parenthesis are the minimum and maximum values.
671 This table is in g km^{-1} opposed to g kg-fuel^{-1} in Table 1.

672

673

674

675

676

677

678

679

680

681

682

683

684 Figure 1:

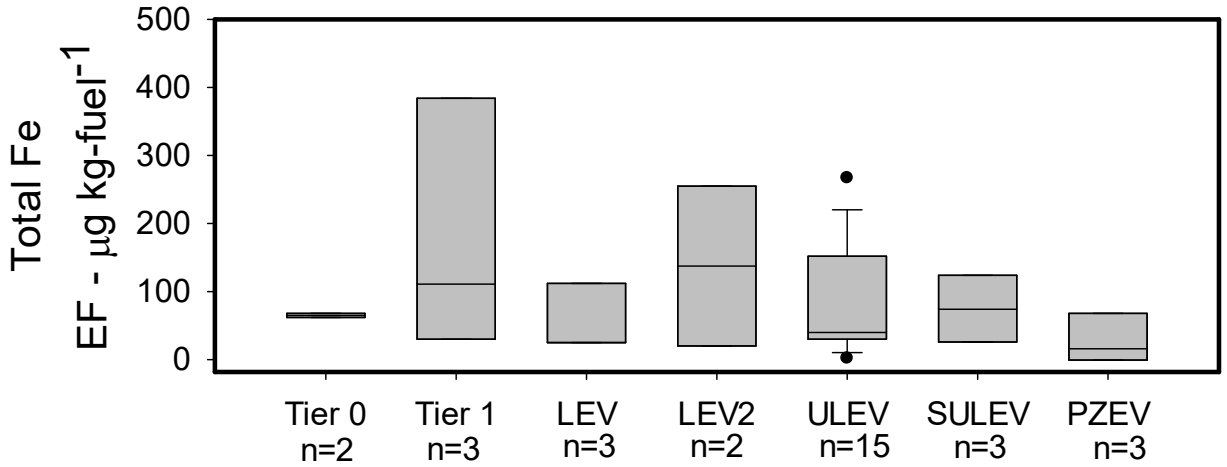

685

686

687

688

689

690

691

692

693

694

695

696

697 Figure 2:

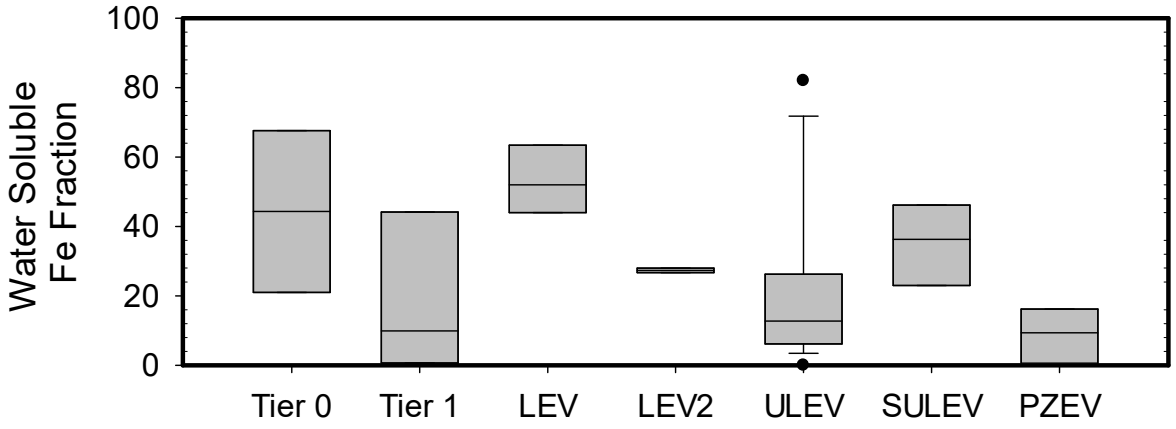

698

699

700

701

702

703

704

705

706

707

708

709

Figure 3:

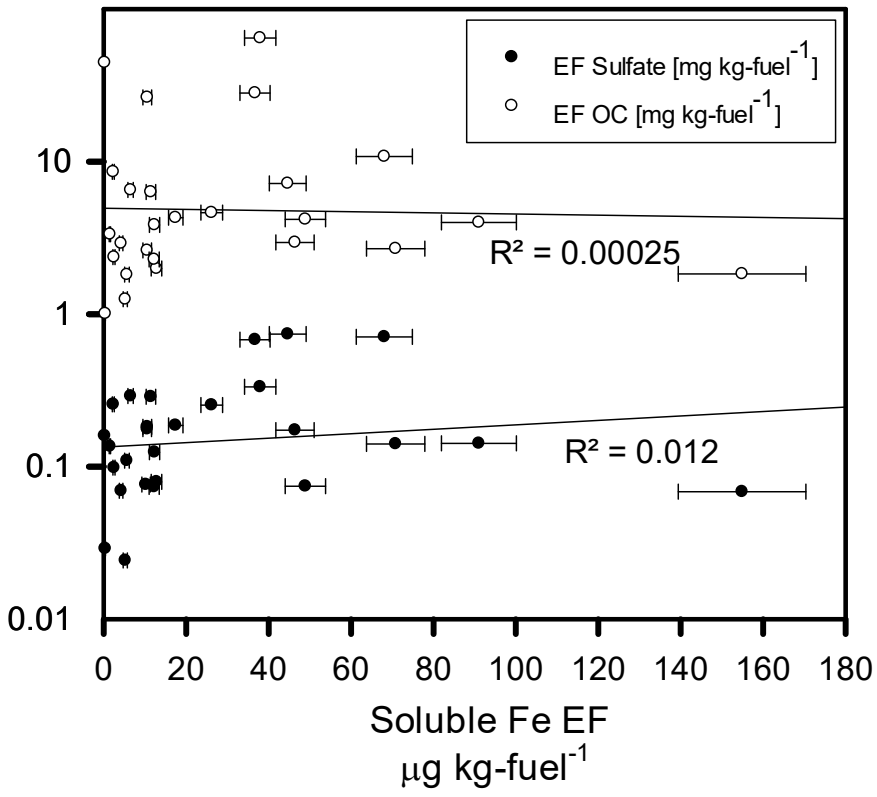
EF Sulfate [mg kg-fuel-1]
EF OC [mg kg-fuel-1]
R² = 0.00025
R² = 0.012
10
1
0.1
0.01
0
20
40
60
80
100
120
140
160
180
Soluble Fe EF
μg kg-fuel-1

719 Figure 4:

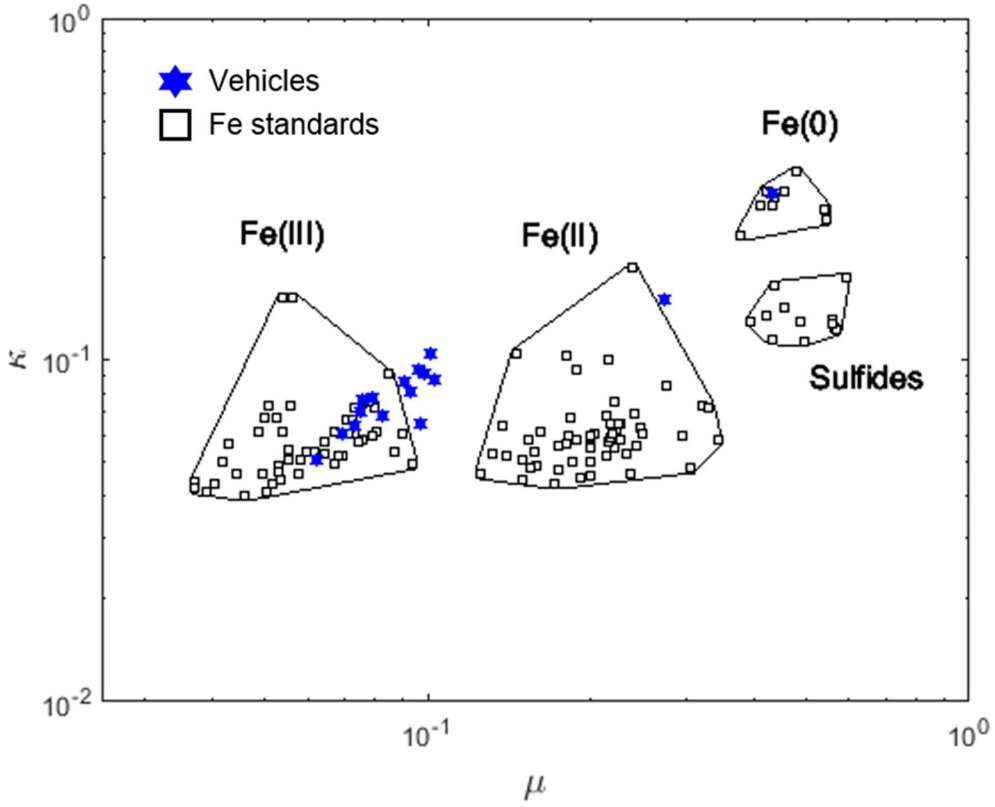

720

721

722

723

724

725

726

727

728

729 Figure 5:

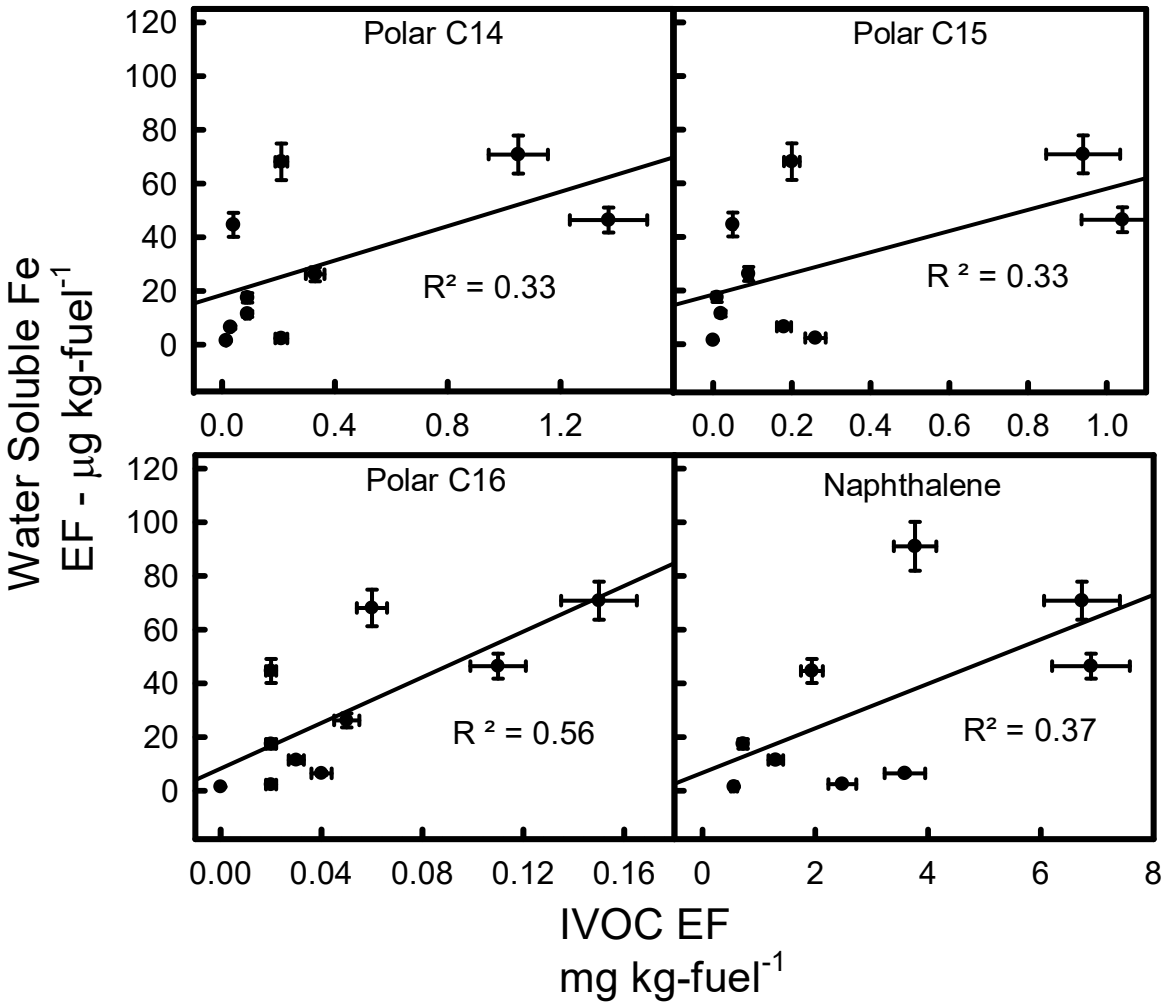

730

731

732

733

734

735

736

737 Figure 6:

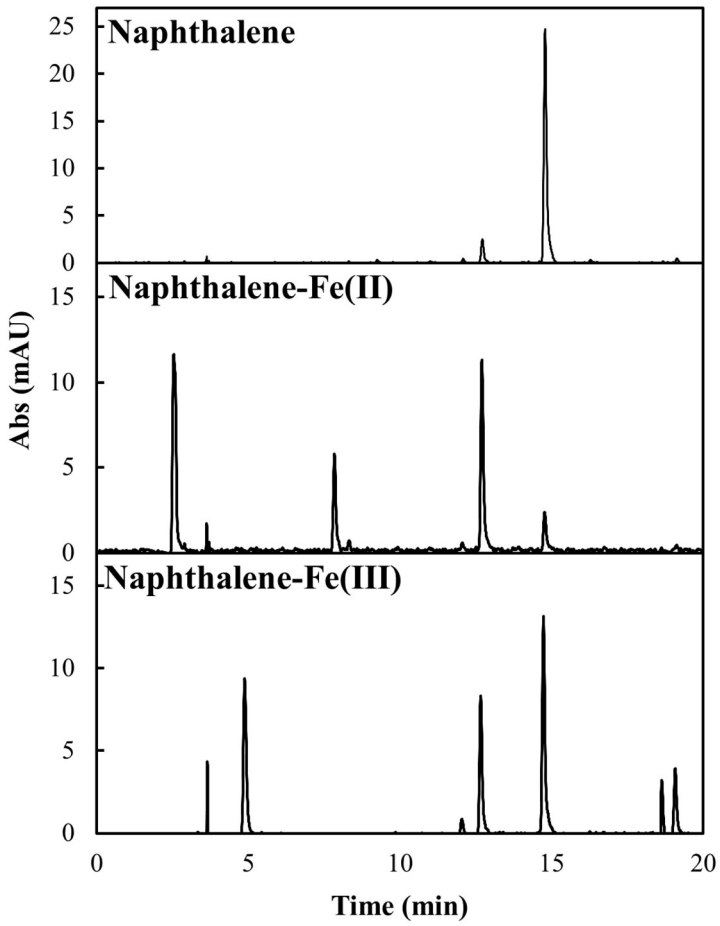

738

739

740

741

742

743

744

745

746

747 Table 1:

	Total Elements	Water-Soluble Elements
Trace elements (μg kg-fuel^{-1})		
Na	50 (0, 200)	30 (0, 100)
Mg	40 (0, 200)	8 (0, 60)
Al	100 (0, 2000)	20 (0, 100)
K	20 (0, 100)	20 (0, 100)
Ca	200 (0, 1000)	200 (0, 1000)
Ti	1 (0, 60)	0.2 (0, 2)
V	0.02 (0, 0.7)	0.02 (0, 0.7)
Cr	5 (0.04, 20)	0.6 (0, 4)
Mn	2 (0.02, 10)	1 (0.007, 8)
Fe	80 (0, 400)	20 (0, 200)
Co	0.2 (0, 1)	0.04 (0, 0.7)
Ni	5 (0, 30)	2 (0, 10)
Cu	20 (0, 200)	20 (0, 100)
Zn	60 (0, 300)	40 (0, 300)
As	0.006 (0, 0.03)	0.006 (0, 0.03)
Se	0.3 (0, 2)	0.05 (0, 0.5)
Rb	0.2 (0, 0.5)	0.01 (0, 0.1)
Sr	1 (0.01, 4)	0.6 (0.003, 3)
Mo	5 (0, 20)	3 (0.002, 30)
Rh	0.06 (0, 0.5)	0.007 (0, 0.1)
Pd	0.8 (0, 6)	0.3 (0, 4)
Ag	0.1 (0, 2)	0.03 (0, 0.5)
Cd	0.007 (0, 0.3)	0.009 (0, 0.05)
Sb	0.2 (0, 1)	0.1 (0, 0.9)
Cs	0.005 (0, 0.02)	0.002 (0, 0.02)
Ba	5 (0, 20)	3 (0.06, 20)
Ce	4 (0, 40)	0.4 (0, 2)
Pt	0.04 (0, 0.4)	0.01 (0, 0.2)
Pb	0.4 (0, 7)	0.3 (0, 7)
U	0.002 (0, 0.03)	0.002 (0, 0.03)

748

749

750

751

752

753 Table 2:

	This study Gasoline (n = 32)	Gasoline(Schauer et al., 2002) (n=9)	Gasoline(Norbeck et al., 1998) (n=40)	Diesel(Norbeck et al., 1998) (n=19)
Fleet Age	1990-2014	1981-1994	1972-1990	1977-1993
PM components (mg km^{-1})				
OC	1 (0.06, 10)	3.3 ± 0.21	16 ± 32	150 ± 330
EC	10 (0.06, 100)	0.77 ± 0.023	3.5 ± 4.8	160 ± 100
sulfate	0.02 (0.001, 0.1)	0.08 ± 0.16	0.93 ± 1.9	0.77 ± .93
Trace elements (μg km^{-1})				
Ag	0.01 (0, 0.25)	4.5 ± 20	0	0
Al	10 (0, 110)	20 ± 17	19 ± 37	31 ± 75
Ba	0.6 (0, 4.4)	0	0	68 ± 75
Ca	30 (0, 130)	26 ± 8.5	81 ± 120	650 ± 930
Cd	0.00 (0, 0.04)	0	0	0
Co	0.01 (0,0.25)	-	0	0
Cr	0.6 (0.008, 4)	0	0	6.2 ± 12
Cu	3 (0, 27)	0	6.2 ± 6.2	19 ± 31
Fe	10 (0, 62)	8.3 ± 2.3	280 ± 680	830 ± 1000
K	2 (0, 15)	3.0 ± 11.3	0	50 ± 170
Mg	7 (0, 120)	-	25 ± 31	99 ± 200
Mn	0.2 (0.002, 1.3)	0	0	6.2 ± 6.2
Mo	0.5 (0, 3.6)	2.3 ± 6.8	0	6.2 ± 12
Ni	0.6 (0, 5.2)	0	6.2 ± 12	12 ± 18
Pb	0.04 (0, 0.57)	0	25 ± 93	19 ± 62
Sb	0.02 (0, 0.21)	17 ± 39	0	0
Sr	0.1 (0, 0.68)	0.75 ± 2.3	0	0
Zn	7 (0, 37)	14 ± 1.5	110 ± 170	810 ± 1500

754

755

756

757